Single-crystal EPR study and DFT structure of the [Mo(CO)5PPh3]+· radical cation

Sidorenkova Cruz Gonzalez, Elena; Berclaz, Théo; Ndiaye, Bassirou; Jouaiti, Abdelaziz; Geoffroy, Michel

How to cite

SIDORENKOVA CRUZ GONZALEZ, Elena et al. Single-crystal EPR study and DFT structure of the [Mo(CO)5PPh3]+· radical cation. In: Journal of physics and chemistry of solids, 2009, vol. 70, n° 3-4, p. 713–718. doi: 10.1016/j.jpcs.2009.02.010

This publication URL: https://archive-ouverte.unige.ch/unige:3549

Publication DOI: 10.1016/j.jpcs.2009.02.010

Journal of Physics and Chemistry of Solids 70 (2009) 713–718

Contents lists available at ScienceDirect

Journal of Physics and Chemistry of Solids

journal homepage: www.elsevier.com/locate/jpcs

Single-crystal EPR study and DFT structure of the $[Mo(CO)_5PPh_3]^{+\cdot}$ radical cation

Helena Sidorenkova, Théo Berclaz, Bassirou Ndiaye, Abdelaziz Jouaiti, Michel Geoffroy *

Department of Physical Chemistry, 30 quai Ernest Ansermet, University of Geneva, 1211 Geneva, Switzerland

ARTICLE INFO

Article history:
Received 24 September 2008
Received in revised form
4 December 2008
Accepted 18 February 2009

Keywords:
A. Organometallic compounds
C. Density functional theory
D. Electron paramagnetic resonance
D. Radiation damage

ABSTRACT

A radical species characterized by a large g-anisotropy and a clearly resolved hyperfine structure with $^{95/97}$Mo and ^{31}P nuclei is formed, at 77 K, by radiolysis of a single crystal of $Mo(CO)_5PPh_3$. The corresponding EPR signals disappear irreversibly with increasing temperature and the angular dependence of the various coupling constants imply a spin delocalization of ~60% and ~4% on the molybdenum and the phosphorus atoms, respectively and are, *a priori*, consistent with the trapping of a one-electron deficient centre. The ability of DFT to predict the EPR tensors for a 17-electron $Mo^{(I)}$ species is verified by calculating the g-tensor and the various ^{14}N and ^{13}C coupling tensors previously reported by Hayes for $[Mo(CN)_5NO]^{3-}$. Calculations at the B3LYP/ZORA/SOMF level of theory show that, in contrast to $Mo(CO)_5PH_3$, one-electron oxidation of $Mo(CO)_5PPh_3$ causes an appreciable change in the geometry of the complex. The *g*-tensor and the $^{95/97}$Mo and ^{31}P isotropic and anisotropic coupling constants calculated for $[Mo(CO)_5PPh_3]^{+\cdot}$ confirm the trapping of this species in the irradiated crystal of $Mo(CO)_5PPh_3$; they also show that the conformational modifications induced by the electron release are probably hindered by the nearby complexes.

1. Introduction

Transition metal complexes with a 17-electron configuration continue to present considerable interest in both fundamental and applied chemistry [1–4]. These species are invoked as intermediates in many syntheses; some of them, for example, have been proposed as catalysts for olefin metathetical polymerization [5], while metal-centred radicals derived from carbonyl complexes, are frequently used for their exceptional substitutional lability [6–8]. Intense efforts have been devoted to describe the electronic structure of 17-electron Mo complexes [9–11]. Since these compounds can often be produced by electrochemical oxidation of 18-electron species, liquid solution electron paramagnetic resonance (EPR) spectra have been used to provide information about their spin delocalization; however, under these conditions only the isotropic hyperfine constants and the average values of the *g*-tensors can be determined. Frozen solution spectra are more informative; however, when the resonance lines are strongly dependant upon several tensors, some ambiguity exists, since different sets of tensors can lead to similar spectra. Most of these ambiguities disappear if the radical cation can be generated by direct ionization of single crystal of the 18-electron complex since, in this type of experiment, the relative orientation of the various eigenvectors can be determined with precision. Such investigations remain nevertheless rare and, probably due to their poor stability, radical cations formed from molybdenum pentacarbonyl derivatives are not known. This lack of experimental results can, of course, be overcome by using new methods of quantum chemistry to describe the electronic structure of such complexes [12,13]. It is clear, however, that the relevance of these calculations has to be checked by comparison with a well-established structure.

The purpose of the present study is to show that the rather unstable radical cation $[Mo(CO)_5PPh_3]^{+\cdot}$ can be formed and trapped, at 77 K, in a single-crystal matrix and to get insight into its electronic structure. To this end, we will first show that calculations using Density Functional Theory (DFT) are able to predict the EPR tensors, which were determined, many years ago by Hayes, for the radical anion $[Mo(CN)_5NO]^{3-}$ [14]. As far as we know, this complex constitutes, indeed, the single example of a 17-electron Mo complex whose tensors have been obtained from a careful single crystal EPR analysis. We will then show that the *g*-tensor, as well as the ^{31}P and $^{95/97}$Mo hyperfine tensors predicted by DFT for $[Mo(CO)_5PPh_3]^{+\cdot}$ are consistent with those measured at low temperature with an X-irradiated single crystal of $Mo(CO)_5PPh_3$. Moreover, comparison between the optimized structures of $[Mo(CO)_5PPh_3]^{+\cdot}$ and $[Mo(CO)_5PH_3]^{+\cdot}$ will point out the role played by the triphenylphosphine ligand in the electronic structure of the radical cation.

* Corresponding author. Tel.: +41 22 702 6552; fax: +41 22 702 6103.
E-mail address: michel.geoffroy@chiphy.unige.ch (M. Geoffroy).

0022-3697/$ - see front matter © 2009 Elsevier Ltd. All rights reserved.
doi:10.1016/j.jpcs.2009.02.010

2. Experimental

$Mo(CO)_5PPh_3$ was synthesized following an already published procedure [15]. The crystal structure (triclinic) has been reported. [16]. As previously explained, the crystal was glued on a small brass cube with $Y//c^*$ and $a^*//-X$ (the crystallographic axes correspond to the reduced cell) [17]; then it was immersed in liquid nitrogen and exposed at 77 K for 2 h to the radiation of a X-rays tube (PW Phillips tube, tungsten anticathode, 30 kV, 30 mA). Any increase in the temperature of the sample was carefully avoided, the crystal was transferred to a finger dewar, and positioned in the EPR cavity of a Bruker 300 spectrometer (X-band). The angular variation of the EPR signals was measured in steps of 10° in the three reference planes. The g and hyperfine tensors were determined using a second-order perturbation treatment and the results were optimized with a least-squares minimization program [18].

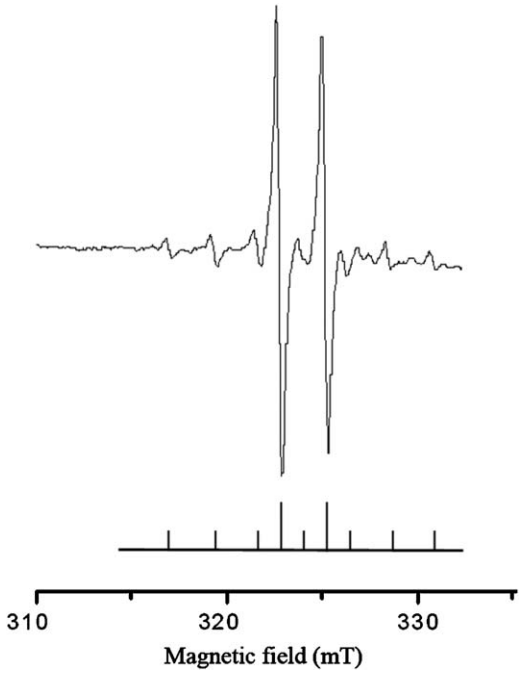

Fig. 1. EPR spectrum recorded at 77 K with a single crystal of $Mo(CO)_5PPh_3$ irradiated at 77 K.

3. Results

3.1. EPR results

Immediately after X-irradiation in liquid nitrogen, a single crystal of $Mo(CO)_5PPh_3$ exhibits, at 77 K, anisotropic EPR signals in the 310–350 mT range (microwave frequency = 9565.1 MHz). An example of spectrum is shown in Fig. 1 (magnetic field oriented in the YZ plane, 10° from the Z-axis). The relative intensities of the signals as well as their angular variations clearly indicate that they are due to a molybdenum centred radical species (^{95}Mo: $I = 5/2$, $g_n = -0.3656$, natural abundance: 15.9%, ^{97}Mo: $I = 5/2$, $g_n = -0.3734$, natural abundance: 9.6%). An additional coupling with a spin $\frac{1}{2}$ nucleus, attributed to ^{31}P, is also observed. The intensity of these signals irreversibly decreases when temperature increases; these lines are no more detected above 180 K.

Analysis of the angular dependence of the signals in the three reference planes (see Electronic Annex 1 in the online version of this article) leads to the g and coupling tensors reported in Table 1. Decomposition of the hyperfine tensors (T) into isotropic (A_{iso}) and anisotropic (τ_{aniso}) components is also given in this table. This decomposition was performed by assuming the signs given in parentheses for the principal values. The ^{31}P–A_{iso} value is considerably smaller than the atomic constant associated to a phosphorus s electron ($A^*_{iso} = 13{,}300$ MHz [19] and indicates an almost negligible phosphorus s-spin density ($\rho_s = 0.005$). Comparing the τ_{max} values with the atomic coupling constants (86 MHz for a Mo d-orbital, 733 MHz for a P p-orbital [19]) leads to a rough estimation of the spin densities: ~60% on molybdenum and 4% on phosphorus.

3.2. DFT calculations

3.2.1. General

The various structures have been optimized with no symmetry constraint, except for $[Mo(CN)_5NO]^{3-}$ (C_4 symmetry), using the Gaussian 03 set of programs [20] and the B3LYP functional [21]. The basis set developed by Stevens et al. [22] and which uses relativistic compact effective potentials was employed for molybdenum, while the standard 6-31+G* basis set was used for the other atoms. Minima were characterized with harmonic frequency calculations (no imaginary frequencies). The EPR properties have been calculated with ORCA [23], a suite of programs, which has been recently used with success for the prediction of g and hyperfine tensors [12,24]. These tensors have been calculated at

Table 1
EPR tensors for species E trapped at 77 K in a single crystal of $Mo(CO)_5PPh_3$.

	Principal values[a]	Eigenvectors			Coupling constants (MHz)	
		/x	/y	/z	A_{iso}	τ_{aniso}
g-tensor	1.961	−0.8827	−0.4020	−0.2429		
	2.080	0.3907	−0.9155	0.0953		
	2.116	0.2608	0.0107	−0.9653		
$^{95/97}$Mo coupling (MHz)	(+)30	0.8440	−0.5330	−0.0650	$A_{iso} = +66$	$\tau_1 = -36$
	(+)52	−0.3270	-0.6060	0.7250		$\tau_2 = -14$
	(+)116	0.4260	0.5900	0.6860		$\tau_3 = +50$
^{31}P coupling (MHz)	(+)54	−0.4791	−0.0406	0.8768	$A_{iso} = 72$	$\tau_1 = -18.5$
	(+)60	0.5729	0.7423	0.3474		$\tau_2 = -12.5$
	(+)103	−0.6649	0.6688	−0.3323		$\tau_3 = +31$

[a] Estimated precision on g-values: ±0.001, on hyperfine values: ±5 MHz.

the optimized geometry using the IGLO-III basis set [25] for the carbon and nitrogen atoms in $[Mo(CN)_5NO]^{3-}$ and for phosphorus in the phosphine containing radical cations; the triple-zeta plus polarization (TZP) basis of Ahlrichs was used for other atoms [26,27] (for Mo: 19s14p9d contracted to 8s6p5d, for H: 5s contracted to 5s, for C and for O: 11s6p1d contracted to 11s6p1d). All basis sets were decontracted. It is well known that for systems containing heavy atoms, a precise calculation of the spin–orbit coupling (SOC) is required to accurately predict the g and hyperfine tensors [28]. For large molecules, however, the treatment of the two-electron part of the SOC is very expensive and several approaches have been proposed to evaluate this interaction. The spin–orbit mean-field (SOMF) treatment, developed by Hess et al. [29], and used for many applications [12,30,31] has recently been implemented in the ORCA program [32] and was used for the present calculations. As demonstrated by van Lenthe et al. scalar relativistic corrections have to be taken into account when calculating EPR properties [33], specially when transition metal are involved. These corrections can be made by applying the zero-order regular approximation (ZORA) [34,35]; they have also been recently implemented in ORCA [12]. In the present study, calculations of the g and hyperfine tensors have been performed without ZORA (set 1), and with ZORA (set 2) at the optimized geometry.

3.2.2. $[Mo(CN)_5NO]^{3-}$

The geometry parameters of $[Mo(CN)_5NO]^{3-}$ has been optimized and is shown in Fig. 2a (see also Electronic Annex 2 in the online version). The corresponding singly occupied molecular orbital (SOMO) is represented in Fig. 2b.

The two sets of calculated EPR tensors together with the experimental data obtained by Hayes [14] from a single-crystal EPR analysis are reported in Table 2.

Table 2
Experimental and DFT predicted EPR tensors for $[Mo(CN)_5NO]^{3-}$.

Tensor	Experimental[a] eigenvalue (orientation)	DFT (set 1)[b]	DFT (set 2)[c]
G			
g_1	1.9736(//Mo–NO)	1.9652	1.9647
g_2	2.0168	2.0109	2.0100
g_3	2.0168	2.0109	2.0100
$^{95/97}$Mo–T (MHz)			
A_{iso}	105.3	83	126
τ_{aniso1}	−28.9	−25	−24
τ_{aniso2}	−28.9	−25	−24
τ_{aniso3}	57.8(//Mo–NO)	50	48
^{14}N–T (NO) (MHz)			
A_{iso}	−8.8	−13	−13
τ_{aniso1}	−2.5	−6	−6
τ_{aniso2}	−2.5	−6	−6
τ_{aniso3}	4.99(//Mo–NO)	12	12
^{14}N–T (CN)eq (MHz)			
A_{iso}	1.54	1	1
τ_{aniso1}	−2.54(//Mo–NO)	−2	−2
τ_{aniso3}	−2.54	−3	−3
τ_{aniso3}	5.08(⊥Mo–(CN)eq)	5	5
^{13}C–T (CN)eq (MHz)			
A_{iso}	33	−31	−33

[a] Values reported in Ref. [14] for $[Mo(CN)_5NO]^{3-}$ trapped in a single crystal of $K_3Co(CN)_6$.
[b] Without ZORA.
[c] With ZORA.

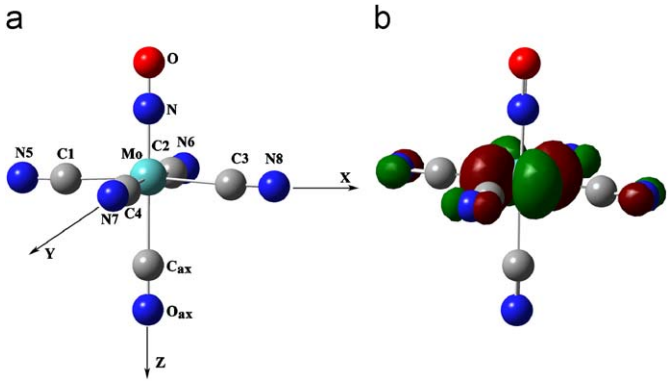

Fig. 2. DFT structure of $[Mo(CN)_5NO]^{3-}$: (a) optimized geometry and (b) three-dimensional representation of the SOMO (isovalue 0.05 a.u.).

3.2.3. $[Mo(CO)_5PH_3]^{+\cdot}$

Apart from a slight increase in the HPH angles, ionization of $Mo(CO)_5PH_3$ hardly changes the angular properties of this complex (see Electronic Annex 3 in the online version). The optimized geometries of the neutral and cationic forms are close to C_s, for both species the Mo–P bond direction is perpendicular to the plane containing the atoms Mo, C1, C2, C3, C4. Formation of the cation causes elongations of the Mo–C ($\delta = 0.08$ Å for C_{ax}, 0.04 Å for C_{eq}) and Mo–P ($\delta = 0.05$ Å) bonds. The optimized geometry of $[Mo(CO)_5PH_3]^{+\cdot}$ is shown in Fig. 3a and the corresponding SOMO in Fig. 3b. The calculated EPR tensors are given in Table 3.

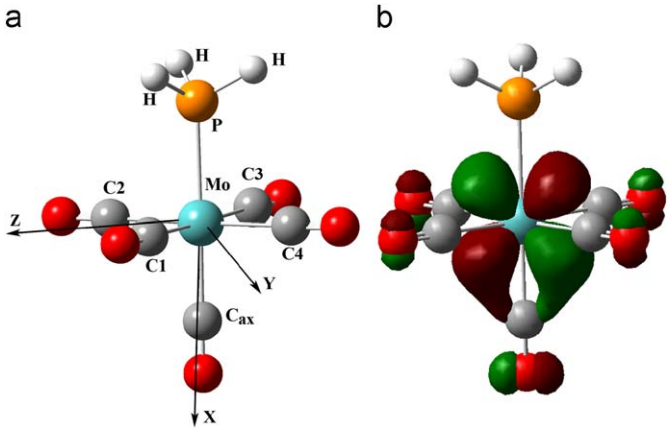

Fig. 3. DFT structure of $[Mo(CO)_5PH_3]^{+\cdot}$: (a) optimized geometry and (b) three-dimensional representation of the SOMO (isovalue 0.05 a.u.).

3.2.4. $[Mo(CO)_5PPh_3]^{+\cdot}$

Optimized geometries of $Mo(CO)_5PPh_3$ and $[Mo(CO)_5PPh_3]^{+\cdot}$ show that ionization of the neutral complex provokes appreciable geometrical changes (see Electronic Annex 4 in the online version). Although the $Mo(CO)_5$ moiety is a regular square base pyramid in both the neutral and cationic species, a 12° tilt of the Mo–P bond in the bisector of the C1MoC2 angle accompanies the oxidation process and the C_{ax}MoP angle decreases from 178.1° to 165.1°. In the resulting structure of the cation, the pyramidality of the Ph_3P ligand has decreased (ΣCPC increases from 309° to 319°) and one of the Mo–P–phenyl bond angles (thereafter ring A) is

Table 3
DFT predicted g-tensors and hyperfine couplings (MHz) for $[Mo(CO)_5PH_3]^{+\cdot}$.

Tensor	DFT (set 1)[a]	DFT (set 2)[b]
g		
g_1	1.9971	1.9971
g_2	2.2576	2.2447
g_3	2.2961	2.2816
$^{95/97}$Mo–T		
A_{iso}	54	82
τ_{aniso1}	−33	−31
τ_{aniso2}	−10	−9
τ_{aniso3}	43	40
^{31}P–T		
A_{iso}	−66	−72
τ_{aniso1}	3	4
τ_{aniso2}	1	1
τ_{aniso3}	−4	−5

[a] Without ZORA.
[b] With ZORA.

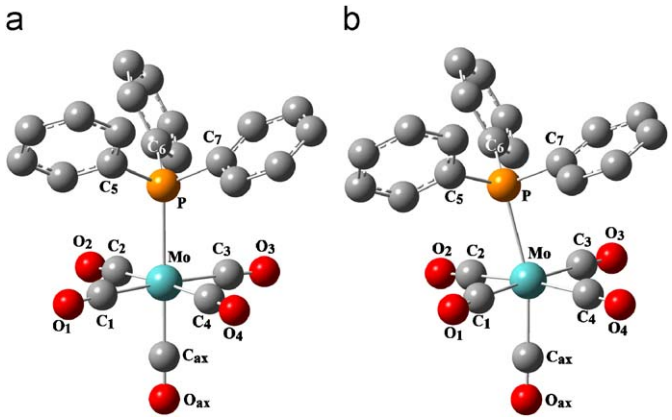

Fig. 4. Optimized geometries (a) of $Mo(CO)_5PPh_3$ and (b) of $[Mo(CO)_5PPh_3]^{+\cdot}$.

Table 4
DFT predicted g-tensors and hyperfine couplings (MHz) for $[Mo(CO)_5PPh_3]^{+\cdot}$.

Tensor	DFT (set 1)[a]	DFT (set 2)[b]
g		
g_1	1.9931	1.9930
g_2	2.0733	2.0752
g_3	2.1226	2.1240
$^{95/97}$Mo–T		
A_{iso}	32	51
τ_{aniso1}	−28	−28
τ_{aniso2}	−10	−10
τ_{aniso3}	39	38
^{31}P–T		
A_{iso}	80	64
τ_{aniso1}	−23	−20
τ_{aniso2}	−20	−16
τ_{aniso3}	43	36

[a] Without ZORA.
[b] With ZORA.

particularly small (Mo–P–C5 = 100°, while Mo–P–C6 and Mo–P–C7 are equal to 117° and 119°, respectively). Moreover, the formation of the cation causes a small shortening of the Mo–P and P–C bonds. The optimized geometries for the neutral and oxidized complexes are visualized in Fig. 4a and b.

The various EPR tensors calculated for $[Mo(CO)_5PPh_3]^{+\cdot}$ are given in Table 4

4. Discussion

Our first objective is to verify that DFT calculations are able to predict the EPR tensors of a Mo(I) complex trapped in a crystal matrix. As reported by Hayes [14], one-electron oxidation of the Heide-Hofman cyanide leads to $[Mo(CN)_5NO]^{3-}$, which could be incorporated in single crystals of $K_3Co(CN)_6$. Remarkably, this author could determine not only the g and Mo coupling tensors for this radical anion but he could also measure hyperfine interactions with the ligands: ^{14}N coupling tensors for NO and for the CN groups located in equatorial positions, as well as the ^{13}C isotropic coupling constant for these latter groups. As shown in Table 2, DFT calculations reproduce the main properties of the experimental g-tensor: axial symmetry, with $g_{\parallel}\sim1.97$ aligned along the Mo–NO bond direction, and $g_{\perp}\sim2.01$. The anisotropic ^{95}Mo coupling constants are also quite consistent with the EPR measurements and confirm that the parallel component, close to 50 MHz, is aligned along $g_{\parallel}$. The predicted isotropic coupling constant (83 MHz), slightly smaller than the experimental value (105 MHz) when the relativistic effects are not included in the calculations, becomes slightly larger than $A_{iso,\ experimental}$ when ZORA is used (126 MHz). Taking into account the line-width of the EPR signals and the small dependence of the EPR parameters upon the host matrix (the g-values measured in a crystal of KBr are slightly different: $g_1 = 1.969$, $g_2 = 2.021$, $g_3 = 2.021$), the accord between experimental and DFT results for g and the ^{95}Mo couplings can be considered as very satisfactory. As shown in Fig. 2b, these g and ^{95}Mo properties reflect the large contribution of the d_{xy} molybdenum atomic orbital to the SOMO. It is worthwhile mentioning the good accord between the experimental and calculated couplings with the ligands. For the NO group, the EPR and DFT values indicate a Fermi contact interaction close to −10 MHz and an anisotropic coupling component ^{14}N–τ_{max} (NO) oriented parallel to the $g_{\parallel}$ direction. The small difference in the ^{14}N–T values probably reflects some uncertainty in the experimental values since the corresponding hyperfine splittings could be measured for only two orientations of the crystal [14]. For the CN groups in equatorial position, experimental and calculated ^{14}N isotropic couplings are very small (~2 MHz) and the ^{14}N–τ_{max} (CN)eq eigenvectors are aligned perpendicular to the Mo–CN bond directions. As shown by the SOMO (Fig. 2b), such an alignment results from the overlap between the Mo d_{xy}-orbital and the corresponding nitrogen p-orbital (e.g. p_y for N8). Finally, the calculated isotropic ^{13}C coupling constants with the (CN)eq groups perfectly agree with the measured value although the positive sign previously proposed for these couplings appears to be negative. Clearly, the good agreement between experimental and calculated parameters obtained for $[Mo(CN)_5NO]^{3-}$ shows that DFT calculations safely predict the structure of hexa-coordinated Mo(I) complexes; we will now use the DFT calculations on $[Mo(CO)_5PPh_3]^{+\cdot}$ (Table 4) to identify the above-mentioned signals E (Table 1).

Comparison between the two sets of values (Tables 1 and 4) reveals a good accordance between experimental and calculated hyperfine constants with ^{95}Mo and ^{31}P nuclei. Taking the effect of the line-width on the experimental precision into account, this agreement can be considered as very satisfactory for both the

Table 5
Orientations of the EPR eigenvectors in $[Mo(CO)_5PPh_3]^{+\cdot}$.

Angles (degrees)	EPR measurement[a]	DFT calculations[b]
(Mo–P, g_{min})	87	87
(Mo–P, Mo–τ_{max})	74	88
(Mo-P, ^{31}P–τ_{max})	23	10
($^{95/97}$Mo–τ_{max}, ^{31}P–τ_{max})	83	88
(g_{min}, $^{95/97}$Mo–τ_{max})	38	49
(g_{min}, ^{31}P–τ_{max})	66	88

[a] Mo–P direction determined for $Mo(CO)_5PPh_3$ (crystallographic direction), eigenvectors obtained from the EPR analysis.
[b] Mo–P direction and eigenvectors determined for the optimized geometry of $[Mo(CO)_5PPh_3]^{+\cdot}$.

isotropic (A_{iso}) and the anisotropic (τ_{aniso}) coupling constants. The experimental as well as the calculated *g*-tensors are characterized by an eigenvalue g_{min} inferior to the free electron values and by two "pseudo-perpendicular" components around 2.1. The experimental g_{min} value is smaller than the calculated value but is not in conflict with the attribution of signals E to the $[Mo(CO)_5PPh_3]^{+\cdot}$ species.

In $[Mo(CO)_5PH_3]^{+\cdot}$ the square base bipyramid structure of the complex is retained; the three eigenvectors $g_{intermediate}$, $^{95.97}$Mo–τ_{max} and ^{31}P–τ_{aniso1} are aligned in the equatorial plane along the bisector of C2MoC3. The pseudo parallel component, g_{min}, lies in the bisector plane of C3MoC4, and makes an angle of 12.8° with the equatorial plane. When PH_3 is replaced by PPh_3, the g_{min} eigenvector makes an angle of 71° with the C1–C4 direction and lies close to the plane containing the C1, C2, C3 and C4 atoms. The normal to this plane makes a small angle with the ^{31}P–τ_{max} eigenvector (7°), and is perpendicular to the Mo τ_{max}-direction (86°).

As mentioned above, DFT calculations show that ionization of $Mo(CO)_5PPh_3$ causes some changes in the geometry of the complex: a reorientation of the PPh_3 group occurs and, in the resulting cation, the phosphorus atom is no more located on the normal to the original equatorial plane. The tilt angle of the Mo–P direction remains nevertheless small (~12°), and if our interpretation is correct the relative orientation of the Mo–P direction and of the EPR eigenvectors calculated by DFT for $[Mo(CO)_5PPh_3]^{+\cdot}$ should be rather close to the relative orientation of the measured eigenvectors and of the Mo–P directions determined from the crystal structure of $Mo(CO)_5PPh_3$. These angular properties are reported in Table 5. Since for axial tensors, only the "parallel" directions are accurately determined, the angular values have been calculated for g_{min}, Mo–τ_{max} and ^{31}P–τ_{max}. Clearly there is no serious discrepancy between the DFT and EPR results. An excellent agreement is observed for the inter-eigenvector angle ($^{95/97}$Mo–τ_{max}, ^{31}P–τ_{max}). The accord for (g_{min}, ^{31}P–τ_{max}) and for (g_{min}, $^{95/97}$Mo–τ_{max}) is less satisfactory; probably the *g* tensor is particularly sensitive to the structure constraints caused by the crystal matrix. This effect could also explain the difference between the experimental and the calculated values of g_{min}.

A precise description of the electronic structure of $[Mo(CO)_5PPh_3]^{+\cdot}$ can be obtained from the DFT results. As shown in Fig. 5b, the somewhat complicated shape of the SOMO results from the tilt of the Mo–P bond: this MO is mainly constituted of a bonding combination of the Mo–d_{xz} and of the "original" sp^n lone pair of the phosphorus. A contribution of the phenyl ring A is also clearly visible, it involves a π-orbital, mainly localized on C5, C6 and C7, which, in part, overlaps the phosphorus–molybdenum bonding region of the molecular orbital. Whereas the highest occupied molecular orbital (HOMO) of $Mo(CO)_5PH_3$ is almost

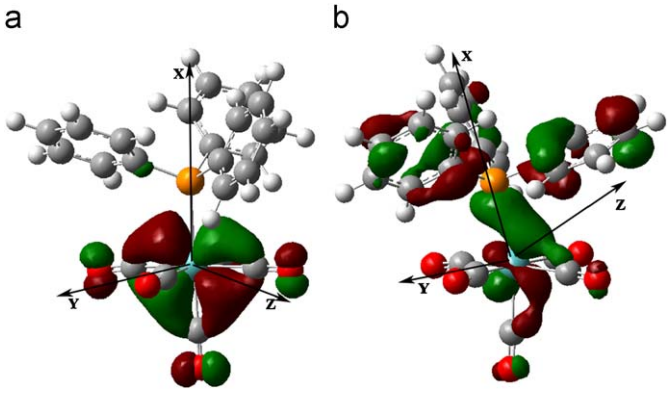

Fig. 5. (a) Representation of the HOMO for $Mo(CO)_5PPh_3$ and (b) representation of the SOMO for $[Mo(CO)_5PPh_3]^{+\cdot}$ (isovalue: 0.04 a.u.).

identical to the SOMO of its cation (Fig. 3b), the HOMO of $Mo(CO)_5PPh_3$ (Fig. 5a), very similar to that of $Mo(CO)_5PH_3$, is clearly different from the SOMO of the radical cation $[Mo(CO)_5PPh_3]^{+\cdot}$ (Fig. 5b). This difference is well reflected by the total spin density on the phosphine ligand, which increases from −0.01 for $[Mo(CO)_5PH_3]^{+\cdot}$ to +0.16 for $[Mo(CO)_5PPh_3]^{+\cdot}$. Moreover, while the one electron-oxidation of $Mo(CO)_5PH_3$ causes an elongation of the Mo–P distance, for $Mo(CO)_5PPh_3$ this oxidation leads to a shortening of this bond.

5. Conclusions

The 17-electron radical cation $[Mo(CO)_5PPh_3]^{+\cdot}$ produced from the exposure of crystalline $Mo(CO)_5PPh_3$ to ionizing radiation could be trapped in the crystal lattice at low temperature. As shown by DFT, in contrast with $Mo(CO)_5PH_3$, ionization of $Mo(CO)_5PPh_3$ alters the conformation of the complex and shortens the Mo–P bond. Although some of these modifications are likely hindered by the neighbour molecules of the crystal lattice, the hyperfine tensors with both the metal and the phosphorus atoms very well agree with the DFT predictions. The g_{min} component, however, seems to be more sensitive to this matrix effect. The constraints of the matrix have probably far less effect on the structure of $[Mo(CN)_5NO]^{3-}$, since in this case the paramagnetic complex was not generated *in situ* in the lattice but was directly incorporated during crystallization.

It is worthwhile mentioning that irradiation of crystals of $Mo(CO)_5PPh_3$ leads to the detection of the main species expected from common mechanisms in radiation chemistry: (1) formation of the radical cation, which is not stable above 100 K, (2) formation of the radical anion, which results from the capture of a thermalized electron by a surrounding neutral molecule; this anion could be detected even after annealing at 300 K [36], (3) formation at room temperature of a radical species due to the homolytic scission of an organic bond; in this case $(CO)_5Mo–PPh_2$ [17].

Acknowledgements

Some of the calculations were performed at the Swiss National Supercomputing Centre. We gratefully acknowledge support from the Swiss National Science Foundation.

Appendix A. Supplementary material

Supplementary data associated with this article can be found in the online version at doi:10.1016/j.jpcs.2009.02.010.

References

[1] W.W. Brennessel, R.E. Jilek, J.E. Ellis, Angew. Chem. Int. Ed. 46 (2007) 6132.
[2] C.D. Hoff, Coord. Chem. Rev. 206 (2000).
[3] M.-H. Delville-Desbois, F. Varret, D. Astruc, Chem. Commun. (1995) 249.
[4] A. Nafady, P.J. Costa, M.J. Calhorda, W.E. Geiger, J. Am. Chem. Soc. 128 (2006) 16587.
[5] M. Tamm, K. Baum, T. Lügger, R. Fröhlich, K. Bergander, Eur. J. Inorg. Chem. (2002) 918.
[6] Z. Lin, M.B. Hall, J. Am. Chem. Soc. 114 (1992) 6754.
[7] Z. Lin, M.B. Hall, Inorg. Chem. 31 (1992) 2791.
[8] M.H. Delville-Desbois, S. Mross, D. Astruc, J. Linares, F. Varret, H. Rabaâ, A. Le Beuze, J.-Y. Saillard, R.D. Culp, D.A. Atwood, A.H. Cowley, J. Am. Chem. Soc. 118 (1996) 4133.
[9] G.M. Aston, S. Badriya, R.D. Farley, R.W. Grime, S.J. Ledger, F.E. Mabbs, E.J.L. McInnes, H.W. Morris, A. Ricalton, C.C. Rowlands, K. Wagner, M.W. Whiteley, J. Chem. Soc. Dalton Trans. (1999) 4379.
[10] J.C. Fettinger, D.W. Keogh, R. Poli, J. Am. Chem. Soc. 118 (1996) 3617.
[11] J.H. MacNeil, A.W. Roszak, M.C. Baird, K.F. Preston, A.L. Rheingold, Organometallics 12 (1993) 4402.
[12] M.M. Cosper, F. Neese, A.V. Astashkin, M.D. Carducci, A.M. Raitsimring, J.H. Enemark, Inorg. Chem. 44 (2005) 1290.
[13] A.C. Saladino, S.C. Larsen, Catal. Today 105 (2005) 122.
[14] R.G. Hayes, J. Chem. Phys. 47 (1967) 1692.
[15] C.N. Matthew, T.A. Magee, J.H. Wotiz, J. Am. Chem. Soc. 81 (1959) 2273.
[16] F.A. Cotton, D.J. Darensbourg, W.H. Isley, Inorg. Chem. 20 (1981) 578.
[17] B. Ndiaye, S. Bhat, A. Jouaiti, T. Berclaz, G. Bernardinelli, M. Geoffroy, J. Phys. Chem. A 110 (2006) 9736.
[18] E.J. Soulié, T. Berclaz, Appl. Magn. Reson. 29 (2005) 401.
[19] J.R. Morton, K.F. Preston, J. Magn. Reson. 30 (1978) 577.
[20] M.J. Frisch, G.W. Trucks, H.B. Schlegel, G.E. Scuseria, M.A. Robb, J.R. Cheeseman, J.A. Montgomery Jr., T. Vreven, K.N. Kudin, J.C. Burant, J.M. Millam, S.S. Iyengar, J. Tomasi, V. Barone, B. Mennucci, M. Cossi, G. Scalmani, N. Rega, G.A. Petersson, H. Nakatsuji, M. Hada, M. Ehara, K. Toyota, R. Fukuda, J. Hasegawa, M. Ishida, T. Nakajima, Y. Honda, O. Kitao, H. Nakai, M. Klene, X. Li, J.E. Knox, H.P. Hratchian, J.B. Cross, C. Adamo, J. Jaramillo, R. Gomperts, R.E. Stratmann, O. Yazyev, A.J. Austin, R. Cammi, C. Pomelli, J.W. Ochterski, P.Y. Ayala, K. Morokuma, G.A. Voth, P. Salvador, J.J. Dannenberg, V.G. Zakrzewski, S. Dapprich, A.D. Daniels, M.C. Strain, O. Farkas, D.K. Malick, A.D. Rabuck, K. Raghavachari, J.B. Foresman, J.V. Ortiz, Q. Cui, A.G. Baboul, S. Clifford, J. Cioslowski, B.B. Stefanov, G. Liu, A. Liashenko, P. Piskorz, I. Komaromi, R.L. Martin, D.J. Fox, T. Keith, M.A. Al-Laham, C.Y. Peng, A. Nanayakkara, M. Challacombe, P.M.W. Gill, B. Johnson, W. Chen, M.W. Wong, C. Gonzalez, J.A. Pople, Gaussian 03, Revision B.03, Gaussian Inc., Pittsburgh, PA, 2003.
[21] (a) A.D. Becke, J. Chem. Phys. 84 (1986) 4524;
(b) A.D. Becke, J. Chem. Phys. 98 (1993) 5648;
(c) C.T. Lee, W.T. Yang, R.G. Parr, Phys. Rev. B 37 (1988) 785.
[22] (a) W.J. Stevens, M. Krauss, H. Basch, P.G. Jasien, Can. J. Chem. 70 (1992) 612;
(b) W. Stevens, H. Basch, J. Krauss, J. Chem. Phys. 81 (1984) 6026;
(c) T.R. Cundari, W.J. Stevens, J. Chem. Phys. 98 (1993) 5555.
[23] F. Neese. ORCA-an ab initio, Density Functional and Semiempirical Program Package, version 2.4, revision 12; Max Planck Institut für Bioanorganische Chemie: Mülheim and der Ruhr, Germany.
[24] S.M. Mattar, J. Phys. Chem. A 111 (2007) 251.
[25] W. Kutzelnig, U. Fleischer, M. Schindler, NMR: Basic Principles and Progress, vol. 23, Springer, Berlin, 1990, p. 165.
[26] A. Schäfer, H. Horn, R. Ahlrichs, J. Chem. Phys. 97 (1992) 2571.
[27] R. Ahlrichs, K. May, Phys. Chem. Chem. Phys. 2 (2000) 943.
[28] (a) A.C. Saladino, S.C. Larsen, J. Phys. Chem. A 107 (2003) 5583;
(b) A.C. Saladino, S.C. Larsen, Catal. Today 105 (2005) 122.
[29] B.A. Hess, C.M. Marian, U. Wahlgren, O. Gropen, Chem. Phys. Lett. 251 (1996) 365.
[30] C.M. Marian, U. Wahlgren, Chem. Phys. Lett 251 (1996) 365.
[31] L. Gagliardi, B. Schimmelpfennig, L. Maron, U. Wahlgren, A. Willets, Chem. Phys. Lett. 344 (2001) 207.
[32] F. Neese, J. Chem. Phys. 122 (2005) 34107.
[33] E. van Lenthe, A. van der Avoird, P.E.S. Wormer, J. Chem. Phys. 108 (1998) 4783.
[34] E. van Lenthe, J.G. Snijders, E. Baerends, J. Chem. Phys. 105 (1996) 6505.
[35] C. Van Wüllen, J. Chem. Phys. 109 (1998) 392.
[36] T. Berclaz, B. Ndiaye, S. Bhat, A. Jouaiti, M. Geoffroy, Chem. Phys. Lett. 440 (2007) 224.